DEUTSCHES ELEKTRONEN – SYNCHROTRON

DESY 91-003
January 1991

Measurement and Analysis of the Reaction $\gamma\gamma \to 3\pi^+3\pi^-$

JADE Collaboration

ISSN 0418-9833

NOTKESTRASSE 85 · D-2000 HAMBURG 52

To be sure that your preprints are promptly included in the
HIGH ENERGY PHYSICS INDEX,
send them to the following (if possible by air mail):

DESY
Bibliothek
Notkestrasse 85
D–2000 Hamburg 52
Germany

DESY 91-003
January 1991

ISSN 0418-9833

Measurement and Analysis of the Reaction $\gamma\gamma \rightarrow 3\,\pi^+\,3\,\pi^-$

JADE Collaboration

R. Pust[2a], J. Olsson[1], J. Allison[5], K. Ambrus[3b], R.J. Barlow[5], W. Bartel[1], S. Bethke[3], C.K. Bowdery[4], S.L. Cartwright[7c], J. Chrin[5], D. Clarke[7], A. Dieckmann[3], I.P. Duerdoth[5], G. Eckerlin[3], E. Elsen[3d], R. Felst[1], A.J. Finch[4], F. Foster[4], T. Greenshaw[2], J. Hagemann[2e], D. Haidt[1], J. Heintze[3], G. Heinzelmann[2], K.H. Hellenbrand[3f], P. Hill[6d], G. Hughes[4], H. Kado[1g], K. Kawagoe[8], C. Kleinwort[2], G. Knies[1], S. Komamiya[3h], H. Krehbiel[1], J. v. Krogh[3], M. Kuhlen[2i], F.K. Loebinger[5], A.A. Macbeth[5], N. Magnussen[1j], R. Marshall[7], R. Meinke[1], R.P. Middleton[7], P.G. Murphy[5], B. Naroska[2], J.M. Nye[4k], F. Ould-Saada[2], D. Pitzl[2l], R. Ramcke[1m], H. Rieseberg[3], A. Sato[8], D. Schmidt[1j], L. Smolik[3d], U. Schneekloth[2d], J.A.J. Skard[6n], J. Spitzer[3], P. Steffen[1], K. Stephens[5], T. Takeshita[8], A. Wagner[3], I.W. Walker[4], G. Weber[2], M. Zimmer[3d], G.T. Zorn[6].

1) Deutsches Elektronen-Synchrotron DESY, Hamburg, Germany.
2) II. Institut für Experimentalphysik der Universität Hamburg, Hamburg, Germany.
3) Physikalisches Institut der Universität Heidelberg, Heidelberg, Germany.
4) University of Lancaster, Lancaster, England.
5) University of Manchester, Manchester, England.
6) University of Maryland, College Park, MD, USA.
7) Rutherford Appleton Laboratory, Chilton, Didcot, England.
8) International Center for Elementary Particle Physics, University of Tokyo, Tokyo, Japan.

a) Now at RWE-DEA AG, Hamburg, Germany.
b) Now at MBB, Munich, Germany.
c) Now at Sheffield University, Sheffield, UK.
d) Now at DESY, Hamburg, Germany.
e) Now at CERN, Geneva, Switzerland.
f) Now at Universität des Saarlandes, Saarbrücken, Germany.
g) Now at Bayer AG, Brunsbüttel, Germany.
h) Now at SLAC, California, USA.
i) Now at MPI, Munich, Germany.
j) Universität-Gesamthochschule Wuppertal, Wuppertal, Germany.
k) Now at ESTEC, Noordwijk, The Netherlands.
l) Now at Santa Cruz, California, USA.
m) Now at Ramcke Datentechnik GmbH, Hamburg, Germany.
n) Now at ST Systems Corporation, Lanham, Maryland, USA.

Abstract

The reaction $\gamma\gamma \rightarrow 3\pi^+3\pi^-$ has been studied using the JADE detector at PETRA. The topological cross section $\sigma(\gamma\gamma \rightarrow 3\,\pi^+\,3\,\pi^-)$ was measured in the CM energy range 1.5 - 5.5 GeV. The production of ρ^0's was observed and the average number of ρ^0's per event measured. The contributions of the subprocesses $\gamma\gamma \rightarrow \rho^0 2\pi^+ 2\pi^-$, $\gamma\gamma \rightarrow \rho^0\rho^0\pi^+\pi^-$ and $\gamma\gamma \rightarrow 3\,\pi^+\,3\,\pi^-$ (phase space) were studied and 95 % C.L. upper limits for the cross section $\sigma(\gamma\gamma \rightarrow \rho^0\rho^0\pi^+\pi^-)$ determined. Finally the Bose–Einstein correlation for pairs of like signed pions was observed. A fit to a standard parametrization gave results consistent with other studies of this effect in pion systems.

1 Introduction

The total hadronic $\gamma\gamma$ cross section is dominated by pion production and the low multiplicity pion systems produced in $\gamma\gamma$ collisions have been intensively studied. So far, both resonance coupling to the $\gamma\gamma$ system and Vector Meson Dominance (VDM) models have been invoked to explain pion production at lower energies, whereas at higher energies, perturbative QCD has been applied [1]. Low multiplicity states seem to result mainly from exclusive resonance production (e.g. $\gamma\gamma \rightarrow f_2(1270) \rightarrow 2\pi, \gamma\gamma \rightarrow a_2(1320) \rightarrow 3\pi$). Higher multiplicity states, on the other hand, have more complex origins, e.g. vector meson pair production in the reactions $\gamma\gamma \rightarrow \rho\rho \rightarrow 4\pi, \gamma\gamma \rightarrow \rho\omega \rightarrow 5\pi$ and $\gamma\gamma \rightarrow \omega\omega \rightarrow 6\pi$.

With increasing multiplicity the detection and measurement of these reactions puts stringent demands on detector hermeticity and reconstruction efficiency. Large integrated luminosities are needed in order to obtain sufficient statistics, since the production rates generally decrease with increasing multiplicity. In the analysis of such multipion systems, combinatorial effects have to be understood in order to unveil the physics of the reactions. For these reasons, first results on the study of exclusive higher multiplicity pion systems produced in $\gamma\gamma$ collisions have only recently been reported [2] and, so far, not more than 7 pions in the final state have been considered.

We report in this paper on an analysis of the reaction

$$\gamma\gamma \rightarrow 3\pi^+3\pi^-, \tag{1}$$

detected in the e^+e^- reaction $e^+e^- \rightarrow e^+e^-\,3\pi^+3\pi^-$. The outgoing electrons were in general produced at small scattering angles and remained undetected in the beampipe (untagged). The experiment was performed using the JADE detector at the PETRA e^+e^- storage ring. The data were taken at an average beam energy of 18.2 GeV and correspond to an integrated luminosity of 221 pb^{-1}. Apart from the topological cross section some details of the final state were studied: the amount of $\rho^0 2\pi^+ 2\pi^-$ and $\rho^0\rho^0\pi^+\pi^-$ production was estimated and the Bose-Einstein correlation of like sign pions was observed and its parameters determined.

Preliminary results on the measurements of the cross section for reaction (1) have been given by the ARGUS collaboration[3]. Recently, the CELLO collaboration presented an analysis of the $3\pi^+3\pi^-$ system, including a study of the ρ^0 content[4,5].

In the following, we describe in section 2 the JADE detector, in section 3 the event selection and in section 4 the measurement of the topological cross section of reaction (1). Section 5 is devoted to the study and measurement of ρ^0 production in the events, including the question

of double ρ^0 production. Finally, section 6 describes the observation and measurement of the Bose-Einstein correlation in the six-pion system. A summary is given in section 7.

2 Detector

The JADE detector has been described in detail elsewhere[6]. Here we mention only those features of the detector that were essential to the present analysis. Charged particles were detected in the central jet chamber with a momentum resolution of $\sigma_p/p \approx 4\,\%$ for momenta relevant to this analysis (< 2 GeV/c). An additional feature of the central jet chamber was the measurement of the ionization energy loss (dE/dx), which was used for particle identification. Photons were detected in the lead glass calorimeter, which surrounded the central jet chamber and consisted of a central barrel part ($|\cos\theta| < 0.82$) and two end caps ($0.89 < |\cos\theta| < 0.97$). Between the jet chamber and the central barrel part of the calorimeter 42 time of flight (TOF) scintillation counters were situated. They were an important part of the trigger system.

The events used in this analysis were triggered in two steps: In the first step (T1) the signals of the TOF counters and the energy sums from the central barrel part of the lead glass calorimeter were used. The barrel counters were arranged in 30 rings of 84 counters each, thus forming rows parallel to the beam with 30 counters each. Six such rows formed a barrel group which, together with the TOF counter in front of the central 2 rows of the barrel group, constituted a TOF Barrel Group (TBG) element in the trigger. There were 42 such elements. The trigger threshold of the energy sums from the barrel groups was 80 MeV.

No special effort was made to trigger on low mass $3\pi^+3\pi^-$ final states. The recorded events were triggered by one or more of the following T1 trigger conditions:

a) 2 fired TOF counters coplanar with the beam; coplanarity width $\pm$ 1 TOF counter ($\pm$ 224 mrad); no more than 6 fired TOF counters overall.

b) 2 fired TOF counters coplanar with the beam; coplanarity width $\pm$ 3 TOF counters ($\pm$ 524 mrad); no more than 4 fired TOF counters overall.

c) 2 fired TBG elements coplanar with the beam; coplanarity width $\pm$ 2 TOF counters ($\pm$ 374 mrad).

d) 2 fired TBG elements with a minimum distance of 3 TOF counters; no more than 6 fired TOF counters overall.

If at least one of the T1 conditions was fulfilled, the trigger decision was postponed to the next (T2) step of the trigger, which was based on jet chamber hits. At least 2 charged tracks were required, as given by the track trigger logic. In case of the T1 conditions a)-c) these tracks had to be coplanar with the beam, within $\sim$ 262 mrad. It should be pointed out that the trigger conditions a)-c) were designed for the efficient triggering of the annihilation reaction $e^+e^- \to \mu^+\mu^-$ and the veto conditions in a),b) and d), for a maximum number of fired TOF counters, were necessary in order to suppress background from spurious triggers, caused by synchrotron radiation.

3 Event Selection

In the first step of the $3\pi^+3\pi^-$ offline event selection, events with exactly six charged tracks and no photons were selected.

- Accepted charged tracks were required to have at least 8 measured points (of a maximum 48 possible points) in the jet chamber and to have a measured momentum greater than 100 MeV/c. They also had to originate in a fiducial cylinder around the interaction point with radius 20 mm and length $\pm$ 200 mm. Thus events with additional tracks from nuclear interactions in the outer wall of the pressure vessel or in the coil (backscatters) as well as tracks from "curling" electrons from conversions, where the pattern recognition program found tracks either originating outside the fiducial region or having too low momentum or too few hits, were included in the sample. Similarly, tracks which were recognized as belonging to an e^+e^- pair from a conversion, were not included in the track counting.

- A photon was defined to be either a reconstructed e^+e^- pair from a conversion or an energy cluster in the lead glass array to which no charged tracks could be associated. This association sometimes failed due to interactions of the charged particles in the outer wall of the pressure vessel or in the coil, e.g. hard scatterings or nuclear interactions producing secondaries. Since most of the resulting "fake" photons were related to lead glass clusters near the impact position of the track, they could be rejected by the additional requirement that the angular separation of tracks and clusters (measured from the interaction point) was greater than 18°. Clusters consisting of only one lead glass counter were required to have at least 50 MeV reconstructed photon energy (barrel) or at least 45 MeV deposited energy (endcaps)[1].

A total of 2441 events passed these criteria. Further cuts were applied to reduce background:

- It was required that the charged tracks had a dE/dx measurement consistent within 3 σ with the pion hypothesis ($\chi^2 < 9 \cdot \sigma^2_{dE/dx}$). This rejected most of the events with slow charged kaons or protons, as is apparent from Figure 1 a.

- Events with identified secondary vertices from the decay $K^0_S \to \pi^+\pi^-$ were rejected.

- To reject beam-gas events the reconstructed common vertex of the six tracks was required to be within $\pm$ 50 mm of the interaction point along the beam line.

- To reject background from non-exclusive events (i.e. events with additional, undetected final state hadrons or photons), only events with a total transverse momentum squared (p_t^2) less than 0.05 (GeV/c)^2 were accepted. The p_t^2 distribution is shown in Figure 1 b and the cut is indicated.

- The remaining events were visually inspected with the help of a graphics display program. Background events, mainly events with additional, unrecognized tracks, were rejected.

After these cuts 724 events remained.

[1] Due to several corrections, e.g. for shower absorption or for differences in light attenuation at different angles of incidence, the reconstructed photon energy is in general different from the deposited cluster energy.

4 The Topological Cross Section of $\gamma\gamma \to 3\pi^+ 3\pi^-$

The invariant 6π mass distribution ($W_{\gamma\gamma}$) of these 724 events shows a broad enhancement between 2 and 3 GeV/c^2 and falls off at higher values of $W_{\gamma\gamma}$. In a given $W_{\gamma\gamma}$ bin the cross section $\sigma(\gamma\gamma \to 3\pi^+ 3\pi^-)$ was determined according to the relation

$$\sigma(\gamma\gamma \to 3\pi^+ 3\pi^-) = \frac{N_{3\pi^+ 3\pi^-}}{L_{e^+e^-} \langle A(W_{\gamma\gamma}) \rangle \int \frac{dL_{\gamma\gamma}}{dW_{\gamma\gamma}} dW_{\gamma\gamma}}, \qquad (2)$$

where $\langle A(W_{\gamma\gamma}) \rangle$ is the average detection efficiency obtained from the Monte Carlo (MC) simulation and $L_{e^+e^-}$ is the integrated luminosity measured with Bhabha events in a previous analysis[7]. $N_{3\pi^+3\pi^-}$ is the number of observed events, after background subtraction as described below. The integration of the $\gamma\gamma$ luminosity function $L_{\gamma\gamma}$, i.e. the simulation of the process $e^+e^- \to e^+e^- X$, was done using the program of ref. [8]. The decay $X \to 3\pi^+3\pi^-$ was simulated according to isotropic phase space using the SAGE program[9]. Production of ρ^0 mesons was taken into account by weighting the events with the matrix elements for $\rho^0 2\pi^+ 2\pi^-$ and $\rho^0\rho^0\pi^+\pi^-$, corresponding to the ρ^0 production rate measured in the data (see section 5). The resulting MC events were passed through a detector simulation program, and were reconstructed and selected using the same programs as were used for the real data. Several corrections were applied in order to take into account features not normally included in the standard JADE detector simulation. These corrections, which are important for low multiplicity, low energy final states, concerned the TOF trigger simulation and interactions of pions in the detector material. The loss of events due to fake photons from pion interactions in the outer wall of the pressure vessel or in the coil was estimated from a study of $3\pi^+3\pi^-1\gamma$ and $3\pi^+3\pi^-2\gamma$ samples.

The background contributions from the processes $\gamma\gamma \to 3\pi^+ 3\pi^- \pi^0$ and $\gamma\gamma \to K^0_S K^0_S \pi^+\pi^-$ were determined from a simulation of these processes assuming cross sections as measured by the ARGUS collaboration[10,11]. The $3\pi^+3\pi^-\pi^0$ contribution was estimated to be 11 %. The $K^0_S K^0_S \pi^+\pi^-$ background is dominant for $W_{\gamma\gamma} < 2$ GeV and can be neglected at higher $W_{\gamma\gamma}$. Further background sources which were considered are other incompletely reconstructed multi-pion final states and channels with charged kaons[12].

Various sources of systematic errors were investigated. These are:

- Determination of the integrated luminosity (3 %).
- Inaccuracies in the MC simulation, investigated by variation of the cuts (5 %).
- Uncertainties in the corrections for fake photons (5 %).
- Uncertainties in the corrections for nuclear interactions (6 %).
- Uncertainties in the background estimation (3 %).

Combining these in quadrature gives an overall systematic error of 13 %. An exception is the $W_{\gamma\gamma}$ bin 1.8–2.0 GeV with a systematic error of 17 % , due to the large error of the dominant $K^0_S K^0_S \pi^+\pi^-$ background.

The resulting values of the cross section $\sigma(\gamma\gamma \to 3\pi^+ 3\pi^-)$ are given in Table 1 and are graphically displayed in Figure 2. A steep rise of the cross section to a maximal value between 2 and 3 GeV is seen, followed by a decrease at higher $W_{\gamma\gamma}$ values. In Figure 3 our result is

compared to the recent measurement by the CELLO collaboration[4]. It can also be compared to the preliminary ARGUS result[10]. All three measurements show the same structure. The ARGUS measurements however lie systematically above ours by a factor 2, corresponding to about 2 standard deviations of the large ARGUS errors. The CELLO data points fall between ours and the ARGUS points and are statistically consistent with both measurements. Note that only statistical errors are shown in Figure 3 and the overall systematic error of 13% for both our and CELLO's measurements should not be forgotten. No systematic error has been given for the ARGUS points.

5 ρ^0 Production in the $3\pi^+3\pi^-$ Channel

The mass distributions of the $\pi^+\pi^-$ combinations in Figure 4 exhibit clear ρ^0 signals. Before the quantitative analysis of these signals is described, an overview of the MC simulation of the ρ^0 production is given.

5.1 Monte Carlo Simulation of ρ^0 Production

The following processes contribute to the production of a $3\pi^+3\pi^-$ final state:

$$\begin{aligned} &a) \quad \gamma\gamma \to 3\pi^+ 3\pi^- \quad \text{phase space (PS)} \\ &b) \quad \gamma\gamma \to \rho^0 2\pi^+ 2\pi^- \\ &c) \quad \gamma\gamma \to \rho^0\rho^0\pi^+\pi^- \end{aligned} \qquad (3)$$

The reaction $\gamma\gamma \to 3\rho^0$ is excluded because of C-parity conservation. Simulation of the processes $\gamma\gamma \to \rho^0 2\pi^+ 2\pi^-$ and $\gamma\gamma \to \rho^0\rho^0\pi^+\pi^-$ was done by weighting non-resonant events with a factor $w = |M|^2$, where the matrix element M contains the Breit-Wigner parametrization[13]:

$$BW_{ij} = \frac{1}{\pi} \frac{\sqrt{m_\rho \Gamma_\rho \, m_{ij}/p^*}}{m^2_\rho - m^2_{ij} - i m_\rho \Gamma_\rho} \qquad (4)$$

$$\Gamma_\rho(m_{ij}) = \Gamma^0_\rho \left(\frac{p^*}{p^*_\rho}\right)^3 \frac{2 p^{*2}_\rho}{p^{*2} + p^{*2}_\rho}, \qquad (5)$$

with $p^* = \sqrt{m^2_{ij} - 4m^2_\pi}$, $p^*_\rho = \sqrt{m^2_\rho - 4m^2_\pi}$ and $m_\rho = 770\,\text{MeV}, \Gamma^0_\rho = 153\,\text{MeV}$[14]. m_{ij} is the invariant mass of the $\pi^+_i\pi^-_j$-combination ($i,j = 1,2,3$). The assumption that the phases of all Breit-Wigner amplitudes are uncorrelated, i.e. the *incoherent* case, leads to the following weights:

$$w^{INCOH}_{\rho 4\pi} = \sum |BW_{ij}|^2 \qquad w^{INCOH}_{\rho\rho\pi\pi} = \sum_{i,j\neq k,l} |BW_{ij}\, BW_{kl}|^2 . \qquad (6)$$

Assuming maximal interference of the Breit-Wigner amplitudes , i.e. the *coherent* case, one gets:

$$w^{COH}_{\rho 4\pi} = \left|\sum BW_{ij}\right|^2 \qquad w^{COH}_{\rho\rho\pi\pi} = \left|\sum_{i,j\neq k,l} BW_{ij}\, BW_{kl}\right|^2 . \qquad (7)$$

The interference term in the coherent case leads to an enhancement of the ρ^0 signal. Thus fits to the $\pi^+\pi^-$ mass distributions from MC samples that were coherently weighted with the

$\rho^0 2\pi^+ 2\pi^-$ and $\rho^0\rho^0\pi^+\pi^-$ final states resulted in 1.6 ρ^0's per event in the first case and 2.6 ρ^0's per event in the second.

Incoherent summation is used in the following analysis unless otherwise stated. In [5] it was also found that an analysis performed using coherent summation resulted in an enhanced ρ^0 signal.

5.2 Fits to the $\pi^+\pi^-$ Mass Distribution

In order to determine the ρ^0 production rate, i.e. the average number of ρ^0's per event, fits to the $\pi^+\pi^-$ mass distribution were performed for several $W_{\gamma\gamma}$ bins. Two different fit methods were used:

χ^2 Fit : The data were fitted with the sum of a Breit-Wigner function and a background distribution, derived from the non-resonant MC simulation. The χ^2 function was defined by

$$\chi^2 = \sum_i \frac{(N_i - T_i)^2}{\sigma_i^2} \qquad \text{with } T_i = aU_i + bR_i. \tag{8}$$

In this expression N_i and σ_i are the number of entries and the corresponding error in bin i. U_i is the number of entries in the background distribution and R_i is the Breit-Wigner function value in the bin center. The parameters a and b were calculated by minimizing χ^2 using the program MINUIT[15]. The ρ^0 production rate $< N_\rho >$ then results from the fitted parameter b.

Maximum Likelihood Fit (ML Fit): The data were fitted to MC distributions of $3\pi^+3\pi^-$ phase space and $\rho^0\rho^0\pi^+\pi^-$. The likelihood function was defined by

$$L = \prod_i \frac{e^{-T_i} T_i^{N_i}}{N_i!} \qquad \text{where } T_i = aN_i^{3\pi^+3\pi^-} + bN_i^{\rho\rho\pi\pi} \tag{9}$$

and $N_i^{3\pi^+3\pi^-}$ and $N_i^{\rho\rho\pi\pi}$ are the number of entries in bin i for the relevant MC distributions. The minimization of $-\log L$ was performed using MINUIT. A 3-parameter fit with an additional $\rho^0 2\pi^+ 2\pi^-$ contribution gave unstable results.

The resulting ρ^0 rate $< N_\rho >$ is given in Table 2. The results of both fit methods are consistent and a graphical presentation is given in Figure 4. The χ^2 per degree of freedom has values between 1 and 2.

In three of the four $W_{\gamma\gamma}$ bins considered, $< N_\rho > > 1$ was observed, implying an essential contribution of $\rho^0\rho^0\pi^+\pi^-$ events. This was confirmed by the $m(\pi^+\pi^-)$ vs. $m(\pi^+\pi^-)$ scatterplots, shown in Figure 5. The clear $\rho^0\rho^0$ signals in these plots are reproduced by making the same plots for the MC data from the simulation of the processes in (3).

5.3 The Extended Maximum Likelihood Fit

Finally the contributions of the 3 processes in (3) were determined by a 3-parameter fit using the *extended maximum likelihood* (EML) method. This method has the advantage that the full event information is used. The EML function was defined by

$$L = \prod_i^N \left[P_i \, e^{-\int P_i(\xi_i) d\xi_i} \right]. \tag{10}$$

The product runs over all events in a given $W_{\gamma\gamma}$ bin. The probability of observing N events is given by the factor $e^{-\int P_i(\xi_i) d\xi_i}$. The event probability P_i is a function of the measured variables ξ_i (i.e. the $\pi^+\pi^-$ masses) and the fractions λ_j ($j = 3\pi^+3\pi^-(\mathrm{PS}), \rho^0 2\pi^+ 2\pi^-, \rho^0\rho^0\pi^+\pi^-$):

$$P_i = \sum_j \lambda_j p_j(\xi_i). \tag{11}$$

The definition of the process dependent normalized probability function p_j follows ref.[16]:

$$p_j(\xi_i) \equiv \frac{A(\xi_i)\, d\sigma_j(\xi_i)/d\xi_i}{\int A(\xi_i)\, d\sigma_j(\xi_i)}. \tag{12}$$

Here $A(\xi_i)$ is the efficiency for an event with the variables ξ_i and the differential cross section is given for fixed $W_{\gamma\gamma}$ by

$$d\sigma_j(\xi_i)/d\xi_i = C R_6(\xi_i) w_j(\xi_i), \tag{13}$$

where C is a constant, R_6 denotes the $3\pi^+3\pi^-$ phase space density and $w_j(\xi_i)$ stands for the square of the matrix element of the final state j. The quantities $w_{\rho 4\pi}$ and $w_{\rho\rho\pi\pi}$ were defined in section 5.1 and $w_{3\pi^+3\pi^-} = 1$. Since the integral $\int A(\xi_i)\, d\sigma_j(\xi_i)$ varies slowly with $W_{\gamma\gamma}$, it was calculated in 100 MeV wide $W_{\gamma\gamma}$ bins. The individual value for each event was then obtained by interpolation. Omitting the constant terms, the extended likelihood function becomes

$$\log L' = \sum_i^N \left[\log \left(\sum_j \frac{\lambda_j w_j}{\int A(\xi_i)\, d\sigma_j(\xi_i)} \right) - \sum_j \lambda_j \right]. \tag{14}$$

The fit parameters λ_j were calculated using MINUIT.

The fit procedure was tested extensively. Samples of simulated MC events with mixtures of the various processes were generated and then fitted in the same manner as the data. These tests showed that for $W_{\gamma\gamma} > 3\,\mathrm{GeV}$ the input mixtures were reproduced within the errors. However, at lower $W_{\gamma\gamma}$, discrepancies of 1-2 standard deviations occurred. In this region the fitted number of ρ^0s was too small. The origin of this systematic deviation is not known, but it must be taken into account that, especially for $W_{\gamma\gamma} < 3\,\mathrm{GeV}$, the final states $\rho^0 2\pi^+ 2\pi^-$ and $\rho^0\rho^0\pi^+\pi^-$ are hard to distinguish. The MC tests also showed that even at low $W_{\gamma\gamma}$ the input mixture was reproduced qualitatively, i.e. abnormal situations, in which one contribution was eliminated, did not occur.

The fit results obtained with incoherent and coherent weights are given in Table 3. Figure 6 shows a graphical presentation[2] of the fit results obtained with incoherent weights. Using coherent instead of incoherent weights leads to a larger yield of $\rho^0 2\pi^+ 2\pi^-$ events and a corresponding loss of $\rho^0\rho^0\pi^+\pi^-$ events. The ρ^0 production rate $< N_\rho >$ evaluated from the EML fit result is given in Table 2. It is, within the large errors, consistent with the result obtained by the two fits to the 1-dimensional mass distribution (see section 5.2), but is systematically lower, as expected from the MC tests described above.

5.4 The reaction $\gamma\gamma \to \rho^0\rho^0\pi^+\pi^-$

If we assume incoherent phases between the Breit-Wigner amplitudes, then the EML fit performed above confirms that ρ^0 production occurs mainly via $\rho^0\rho^0\pi^+\pi^-$. Due to the model

[2] The presentation is due to G. Alexander and A. Klatchko.

dependence in this assumption and the systematic uncertainties mentioned above.we prefer to give only upper limits for the cross section $\sigma(\gamma\gamma \to \rho^0\rho^0\pi^+\pi^-)$ (Table 4). These upper limits were evaluated from the results of the χ^2 fit assuming the $\rho^0 2\pi^+ 2\pi^-$ fraction to be zero. The limits are compared to the CELLO measurements in Figure 7. The results are compatible with each other.

5.5 Discussion of the results

The results from the 1-dimensional χ^2 fit, on the number of ρ^0's as a function of $W_{\gamma\gamma}$, are plotted in Figure 8, where the results of the CELLO collaboration are also shown. The agreement is good. It is interesting to observe that the initial high rate of almost 2 ρ^0's per event at low $W_{\gamma\gamma}$ drops to less than 1 ρ^0 per event between 3 and 4 GeV $\gamma\gamma$ energy. This drop is followed by an increase at higher $W_{\gamma\gamma}$. The results of the EML fit with incoherent weights (Table 3) indicate that at lower $W_{\gamma\gamma}$ values the ρ^0's are mainly due to $\rho^0\rho^0\pi^+\pi^-$ production, while at high $W_{\gamma\gamma}$ also $\rho^0 2\pi^+ 2\pi^-$ production plays a role.

The final state $\rho^0\rho^0\pi^+\pi^-$ could be caused by the production of a vector meson pair, $\gamma\gamma \to \rho^0\rho^0(1700)$, or by a tensor meson pair, $\gamma\gamma \to a_2^+ a_2^-$. The total hadronic $\gamma\gamma$ cross section has been estimated by A. Levy[17,18] in a phenomenological model via the measured cross sections $\sigma(\gamma\gamma \to V^0 V'^0)$, where V^0, V'^0 denote the vector mesons ρ, ϕ, ω, K^*. For $\gamma\gamma$ energies above 2 GeV the model predictions are too low. A possible explanation is the missing $\gamma\gamma \to \rho^0\rho^0(1700)$ contribution. A $\rho\pi\pi$ decay mode has been reported for the $\rho(1700)$ meson. However, the precise nature of the $\rho(1700)$, previously called $\rho(1600)$ or ρ', is by no means clear[14]. It cannot be determined from the present data whether the observed double ρ^0 production is associated with other resonances, like $\rho^0(1700)$, $a_1(1260)$ or $a_2(1320)$. The relevant mass distributions, $(\pi^+\pi^-)_\rho\pi^+\pi^-$ and $(\pi^+\pi^-)_\rho\pi$, do not show resonant structures. The upper limits of the cross section for the reaction $\gamma\gamma \to \rho^0\rho^0(1700)$ (multiplied by the branching ratio for $\rho^0(1700) \to \rho^0\pi^+\pi^-$) are therefore identical to the upper limits given in Table 4. Considering the size of the BR($\rho^0(1700) \to \rho\pi\pi$), these upper limits can accomodate a rate of $\gamma\gamma \to \rho^0\rho^0(1700)$ large enough to give the missing contribution in the total cross section, as discussed in [17].

We note that a further study of this question should involve a spin analysis, preferably in connection with a study of the other charge combinations in a $2\pi^+ 2\pi^- 2\pi^0$ sample.

6 The Bose-Einstein Correlation

The well-known Bose-Einstein correlation[3] between like charged pions is defined by the correlation function, i.e. the ratio of the number of like charged pion pairs N^L to the corresponding number N^{ref} in a reference sample with uncorrelated pions. In the analysis we used the traditional parametrization of the correlation function C in terms of the Lorentz-invariant variable $Q^2 \equiv M^2_{\pi\pi} - 4m^2_\pi$ [20]:

$$C(Q^2) \equiv \frac{N^L}{N^{ref}} = a\left(1 + \lambda e^{-(r)^2 Q^2}\right). \qquad (15)$$

In this expression a is a normalization constant, r is a measure of the space-time dimensions of the pion emission source and λ describes the coherence of the source. λ is 1 for a totally incoherent source.

[3] Also called the GGLP effect after its discoverers [19,20].

Two different reference samples were used:
a) The combinations of unlike sign pions in the data (N_D^U).
b) The like sign pion combinations obtained by the MC simulation, in which the BE effect was not taken into account (N_{MC}^L).
The number of like sign pions N_D^L in the data as function of Q^2 is compared with both reference rates in Figure 9. A clear enhancement at low values of Q^2 becomes visible in the $\pi^\pm\pi^\pm$ data. In the $\pi^-\pi^-$ distribution in reference sample a) an enhancement in the ρ^0 region is also observed. In order to remove the influence of ρ^0 production, the corresponding correlation function has been divided by the ratio N_{MC}^L/N_{MC}^U, where N_{MC}^U is the number of unlike sign pion combinations in the MC simulation. The ratios

$$\text{a)}\ \frac{N_D^L}{N_D^U} \Big/ \frac{N_{MC}^L}{N_{MC}^U} \qquad \text{b)}\ \frac{N_D^L}{N_{MC}^L}$$

are plotted in Figure 10. The curves result from a fit with the parametrization in equation (15). The corresponding results for the parameters λ and r are given in Table 5 with their statistical errors. A comparison of the results obtained with both reference samples shows that systematic errors are of the same order as the statistical errors. The fitted normalization constant a is about 0.9 and $\chi^2/DOF \approx 1$.

Table 5 also contains the result of the previous Mark II analysis[21] for $\gamma\gamma \to$ multihadrons, as well as a recent result from the CELLO collaboration[4] for the channel studied here, $\gamma\gamma \to 3\pi^+ 3\pi^-$. The results are consistent for all $\gamma\gamma$ analyses, with λ values close to 1, indicating a fully incoherent source of like sign pions. Further results of analyses performed with data from e^+e^- annihilation are also given in Table 5. Here λ is systematically lower, indicating a higher degree of coherence. It is interesting to relate this to the difference in production mechanisms: $q\bar{q}$ fragmentation models describe the annihilation data very well, while for the low energy $\gamma\gamma$ produced hadrons, VDM related models provide better descriptions. An exception here is given by the analysis for $e^+e^- \to J/\psi \to$ hadrons, where again λ is close to 1, indicating complete incoherence. We also note that in all cases the size of the source, given by the parameter r, appears to be similar and is of order ~ 0.7 fm.

7 Summary

The reaction $\gamma\gamma \to 3\pi^+ 3\pi^-$ was studied with the JADE detector. The topological cross section $\sigma(\gamma\gamma \to 3\pi^+ 3\pi^-)$ was determined for $\gamma\gamma$ energies between 1.5 and 5.5 GeV. It reaches, after a steep rise, a maximum value of 5 nb between 2 and 3 GeV and then decreases. Measurements of the ARGUS and CELLO collaborations show the same features, however, the preliminary ARGUS measurements lie systematically a few standard deviations higher than ours, ignoring systematic errors.

A large amount of ρ^0 production was observed, with an average of 1.4 ρ^0's per event. Above the threshold for $\rho^0\rho^0\pi^+\pi^-$ production nearly 2 ρ^0's per event were measured, while between 3 and 4 GeV $\gamma\gamma$ energy, a minimum of 0.8 ρ^0's per event was observed. Above 4 GeV the ρ^0 rate increases again, to 1.6 ρ^0's per event.

An analysis using the extended maximum likelihood method showed that at lower $\gamma\gamma$ energies the ρ^0 rate is mainly due to $\rho^0\rho^0\pi^+\pi^-$ production, while at higher energies $\rho^0 2\pi^+ 2\pi^-$

production is also of importance. This result was obtained assuming incoherent addition of interfering ρ^0 amplitudes. Upper limits of the reaction $\gamma\gamma \to \rho^0 2\pi^+ 2\pi^-$ were determined; they are identical to the upper limits for the reaction $\sigma(\gamma\gamma \to \rho^0\rho^0(1700))\cdot BR(\rho^0(1700) \to \rho^0\pi^+\pi^-)$. No indication of $\rho^0(1700)$ or of other resonance production was observed.

Bose-Einstein correlation for like sign pions was observed and fits to the standard correlation function were made. The result is consistent with other measurements of this effect in $\gamma\gamma$ reactions and indicates a fully chaotic source of pions. Similar studies in e^+e^- annihilation data indicate a less chaotic source of pions and a different production mechanism. The size of the source is however similar in both e^+e^- and $\gamma\gamma$ data and is about 0.7 fm.

Acknowledgements

We are indebted to the PETRA machine group and the DESY computer centre staff for their excellent support during the experiment and to all the engineers and technicians of the collaborating institutions who have participated in the construction and maintenance of the apparatus. We gratefully acknowledge discussions with M. Feindt and A. Klatchko, in particular concerning the approach in the analysis of the ρ^0 content. We also thank B. Boštjančič and H. Kolanoski for advice in the use of the EML fitting method. This experiment was supported by the Bundesministerium für Forschung und Technologie, by the Ministry of Education, Science and Culture of Japan, by the UK Science and Engineering Research Council through the Rutherford Appleton Laboratory and by the US Department of Energy. The visiting groups at DESY wish to thank the DESY directorate for the hospitality extended to them.

References

[1] A. Nilsson, Proceedings of the XXIVth Intern. Conf. on High Energy Physics, Eds. R. Kotthaus and J. Kühn, Munich, Germany (1988) 649.
A. Levy, Proceedings of the XXIVth Intern. Conf. on High Energy Physics, Eds. R. Kotthaus and J. Kühn, Munich, Germany (1988) 655.
U. Maor, Proceedings of the VIIIth Intern. Workshop on Photon-Photon Collisions, Ed. U. Karshon, Shoresh, Israel (1988) 282.
A. Nilsson, Proceedings of the VIIIth Intern. Workshop on Photon-Photon Collisions, Ed. U. Karshon, Shoresh, Israel (1988) 261.
M. Ronan, Proceedings of the VIIth Intern. Workshop on Photon-Photon Collisions, Eds. A. Courau and P. Kessler, Paris, France (1986) 51.
Ch. Berger and W. Wagner, Physics Reports **146** (1987).

[2] PLUTO Coll., Ch. Berger et al., Z. F. Phys. **C29**(1985)183.
ARGUS Coll., H. Albrecht et al., Phys. Lett. **196B**(1987)101.
ARGUS Coll., H. Albrecht et al., Phys. Lett. **198B**(1987)255.
ARGUS Coll., reported by A. Nilsson, Proceedings of the VIIIth Intern. Workshop on Photon-Photon Collisions, Ed. U. Karshon, Shoresh, Israel (1988) 21.
CELLO Coll., reported by M. Feindt, Proceedings of the VIIIth Intern. Workshop on Photon-Photon Collisions, Ed. U. Karshon, Shoresh, Israel (1988) 3.

[3] ARGUS Coll., reported by A. Nilsson, in [2].

[4] CELLO Coll., H.-J. Behrend et al., Phys. Lett. **245B** (1990) 298.

[5] CELLO Coll., H.-J. Behrend et al., DESY preprint 90-066, Tel-Aviv Univ. preprint TAUP 1801-90

[6] JADE Coll., W. Bartel et al., Phys.Lett. **88B** (1979) 171, Phys.Lett. **92B** (1980) 206, Phys.Lett. **99B** (1981) 277.

[7] JADE Coll., W.Bartel et al., Phys. Lett. **129B** (1983) 145.

[8] S. Kawabata, Program Write-up (1982), unpublished.
Contribution to the parallel sessions, reported by J.H. Field, Proceedings of the Fourth Intern. Colloquium on Photon-Photon Interactions, ed. G.W. London, Paris (1981) 447.

[9] J. Friedman, Program Write-up SAGE (1972), unpublished.

[10] A. Nilsson, Proc. VIIIth Intern. Workshop on Photon-Photon Collisions, Shoresh (1988), Ed.: U. Karshon, World Scientific (1988) 261.

[11] ARGUS Coll., H. Albrecht et al., Phys. Lett. **212B** (1988) 528.

[12] R. Pust, Diplomarbeit Universität Hamburg 1990, DESY Internal Report F22-90-03.

[13] J.D. Jackson, Nuovo Cim. **34** (1964) 1644.

[14] Particle Data Group, Phys. Lett. **204B** (1988).

[15] F. James, M. Roos, Program Write-up MINUIT (1977), unpublished.

[16] TASSO Coll., M. Althoff et al., Z. Phys. **C16** (1982) 13.

[17] A. Levy; Phys. Lett. **181B** (1986) 401.

[18] A. Levy; Phys. Lett. **215B** (1988) 421.

[19] G. Goldhaber et al., Phys. Rev. Lett. **3** (1959) 181.

[20] G. Goldhaber, S. Goldhaber, W. Lee and A. Pais, Phys. Rev. **120** (1960) 300.

[21] MARK II Coll., I. Juričić et al., Phys. Rev. **D39** (1989) 1.

[22] TASSO Coll., M. Althoff et al., Z. Phys. **C30** (1986) 355.

[23] TPC/2γ Coll., H. Aihara et al., Phys. Rev. **D31** (1985) 996.

$W_{\gamma\gamma}$ [GeV]	$\langle A(W_{\gamma\gamma})\rangle$	$N_{3\pi^+3\pi^-}$	$\sigma_{\gamma\gamma\to 3\pi^+3\pi^-}$ [nb]
1.5 - 1.8	0.012	6± 4	0.7 ± 0.4
1.8 - 2.0	0.024	-15± 11	0.0 ± 1.3
2.0 - 2.2	0.038	37± 10	3.2 ± 0.9
2.2 - 2.4	0.051	66± 10	5.0 ± 0.8
2.4 - 2.6	0.060	64± 10	4.7 ± 0.8
2.6 - 2.8	0.072	73± 10	5.1 ± 0.7
2.8 - 3.0	0.074	62± 9	4.8 ± 0.7
3.0 - 3.2	0.080	54± 8	4.4 ± 0.7
3.2 - 3.4	0.085	33± 7	3.8 ± 0.6
3.4 - 3.6	0.092	32± 6	2.8 ± 0.6
3.6 - 3.8	0.091	27± 6	2.6 ± 0.6
3.8 - 4.0	0.098	28± 6	2.8 ± 0.6
4.0 - 4.2	0.102	23± 5	2.5 ± 0.6
4.2 - 4.4	0.104	17± 4	1.9 ± 0.5
4.4 - 4.6	0.105	8± 3	1.0 ± 0.4
4.6 - 4.8	0.107	7± 3	1.0 ± 0.4
4.8 - 5.0	0.108	4± 2	0.7 ± 0.3
5.0 - 5.5	0.110	11± 3	0.7 ± 0.2

Table 1: Topological cross section for the reaction $\gamma\gamma \to 3\pi^+ 3\pi^-$. The errors are statistical. The overall systematic error is 13%, in the bin 1.8 - 2.0 GeV 17%.

$W_{\gamma\gamma}$ [GeV]	$< N_\rho >$		
	χ^2 fit	ML fit	EML fit (incoh.)
2.1 – 2.6	1.9 ± 0.2	1.7 ± 0.2	1.2 ± 0.6
2.6 – 3.1	1.3 ± 0.2	1.3 ± 0.2	0.7 ± 0.4
3.1 – 4.0	0.8 ± 0.2	0.7 ± 0.2	0.5 ± 0.8
4.0 – 5.5	1.6 ± 0.3	1.8 ± 0.3	1.4 ± 0.7
1.5 – 5.5	1.4 ± 0.1	1.4 ± 0.1	0.9 ± 0.3

Table 2: Average number of ρ^0's per event $< N_\rho >$ as derived from fits to the 1-dimensional $\pi^+\pi^-$ mass distribution and from the extended maximum likelihood fit using incoherent weights.

$W_{\gamma\gamma}$ [GeV]	incoherent			coherent		
	$3\pi^+3\pi^-$	$\rho^0 2\pi^+ 2\pi^-$	$\rho^0\rho^0\pi^+\pi^-$	$3\pi^+3\pi^-$	$\rho^0 2\pi^+ 2\pi^-$	$\rho^0\rho^0\pi^+\pi^-$
2.1 - 2.6	0.34 ± 0.16	0.09 ± 0.29	0.57 ± 0.17	0.33 ± 0.12	0.33 ± 0.22	0.34 ± 0.14
2.6 - 3.1	0.67 ± 0.16	0.00 ± 0.24	0.33 ± 0.12	0.71 ± 0.13	0.13 ± 0.21	0.16 ± 0.12
3.1 - 4.0	0.74 ± 0.24	0.02 ± 0.44	0.24 ± 0.22	0.80 ± 0.13	0.19 ± 0.12	0.00 ± 0.12
4.0 - 5.5	0.00 ± 0.13	0.56 ± 0.24	0.44 ± 0.22	0.15 ± 0.19	0.86 ± 0.30	0.00 ± 0.18

Table 3: Fractions of the different final states, resulting from the extended maximum likelihood fit.

$W_{\gamma\gamma}$ [GeV]	$\sigma(\gamma\gamma \to \rho^0\rho^0\pi^+\pi^-)$ [nb]
2.1 – 2.6	6.0
2.6 – 3.1	4.4
3.1 – 4.0	1.7
4.0 – 5.5	1.6

Table 4: Upper limits for $\sigma(\gamma\gamma \to \rho^0\rho^0\pi^+\pi^-)$ (95 % CL).

Experiment	Process	E_{CM} [GeV]	λ	r [fm]
JADE a) b)	$\gamma\gamma \to 3\pi^+3\pi^-$	$W_{\gamma\gamma}$ = 1.5 – 5.5	1.01 ± 0.16 0.77 ± 0.14	0.67 ± 0.08 0.72 ± 0.10
CELLO[4]	$\gamma\gamma \to 3\pi^+3\pi^-$	$W_{\gamma\gamma}$ = 1.5 – 7.5	0.87 ± 0.24	0.62 ± 0.12
MARK II (SPEAR)[21]	$e^+e^- \to J/\Psi$	3.1	1.00 ± 0.03 ± 0.08	0.81 ± 0.02 ± 0.05
(PEP)[21]	$\gamma\gamma \to X$	$W_{e^+e^-}$ = 29	0.87 ± 0.07 ± 0.07	0.84 ± 0.06 ± 0.05
(SPEAR)[21]	$e^+e^- \to X$	4.1–6.7	0.66 ± 0.04 ± 0.05	0.71 ± 0.04 ± 0.04
(PEP)[21]	$e^+e^- \to X$	29	0.50 ± 0.03 ± 0.04	0.84 ± 0.06 ± 0.05
TASSO[22]	$e^+e^- \to X$	34	0.70 ± 0.06 ± 0.09	0.80 ± 0.06 ± 0.05
TPC/2γ[23]	$e^+e^- \to X$	29	0.61 ± 0.05 ± 0.06	0.65 ± 0.04 ± 0.06

Table 5: Results of the fits to the Bose-Einstein correlation function compared with results of other e^+e^- experiments.

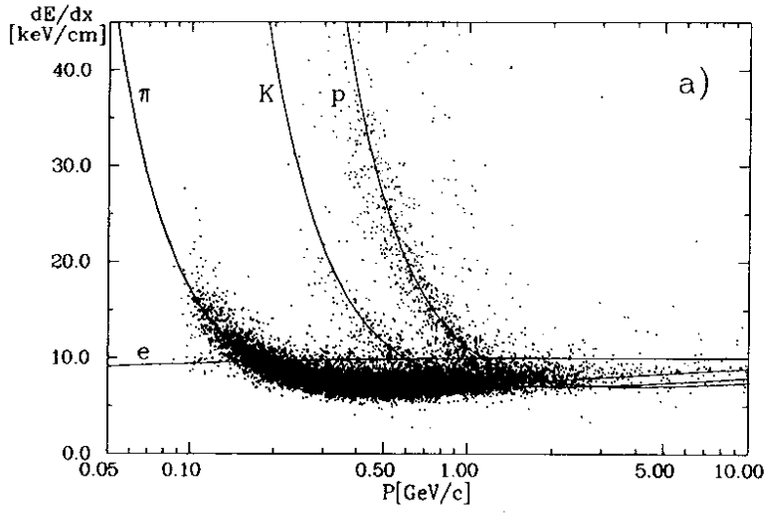

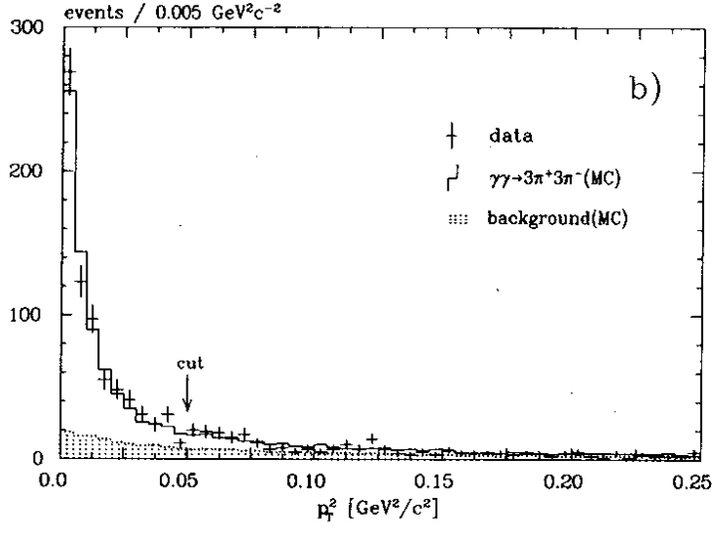

Figure 1: a) Measured energy loss dE/dx for 6 prong events. b) Sum of transverse momenta (squared). The MC distributions result from a fit in which the background was described by $3\pi^+3\pi^-$ events from incompletely reconstructed $3\pi^+3\pi^-\pi^0$ and $4\pi^+4\pi^-$ final states.

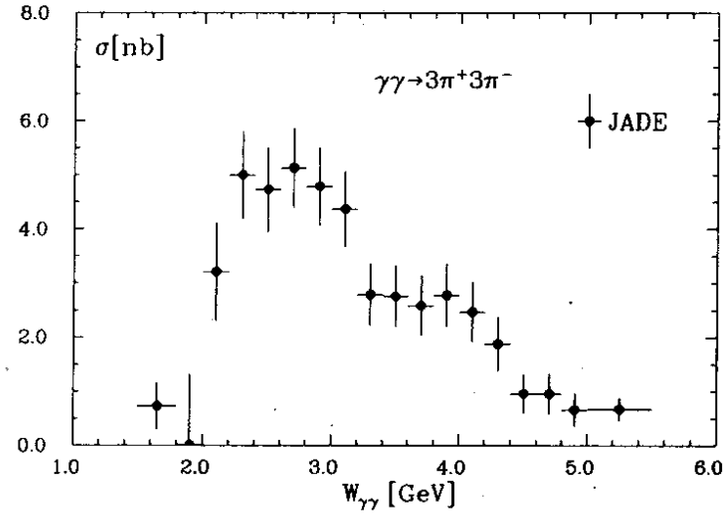

Figure 2: Measured topological cross section.

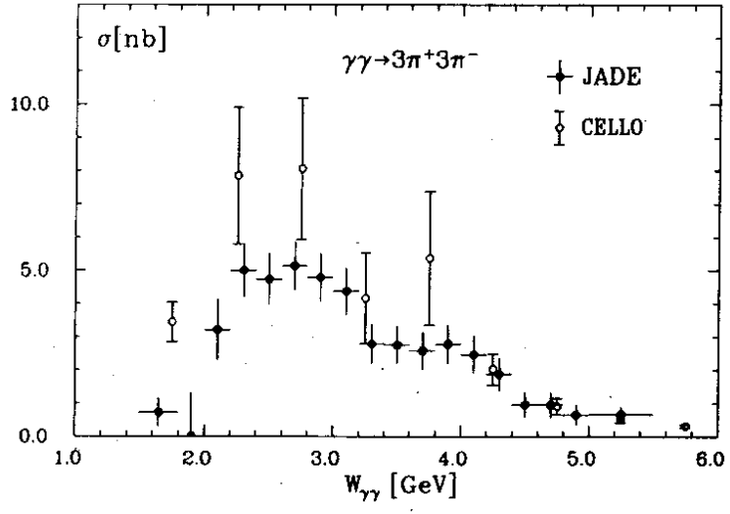

Figure 3: Measured topological cross section compared with the CELLO measurements.

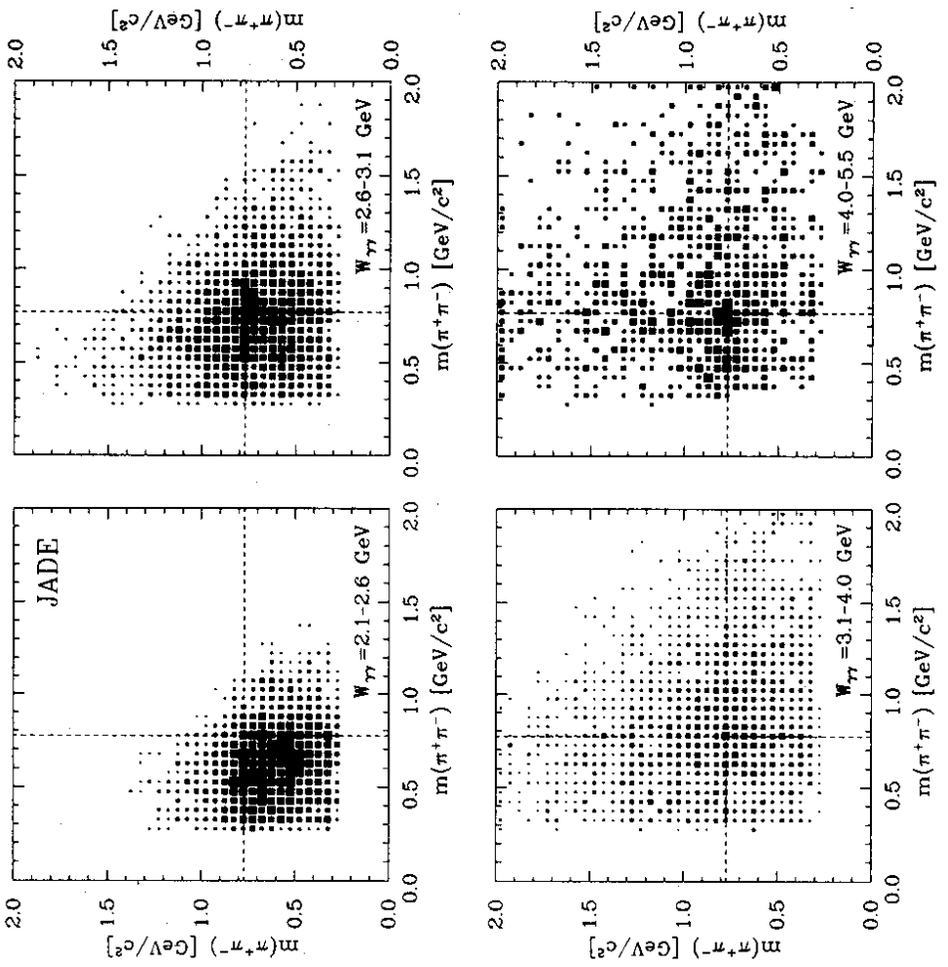

Figure 5: Scatter plots of $m(\pi^+\pi^-)$ vs. $m(\pi^+\pi^-)$ for 4 different $W_{\gamma\gamma}$ bins. There are 18 entries/event. To symmetrize the plots the x- and y-axes were chosen randomly for each entry. The nominal ρ^0 mass is marked by the dashed lines.

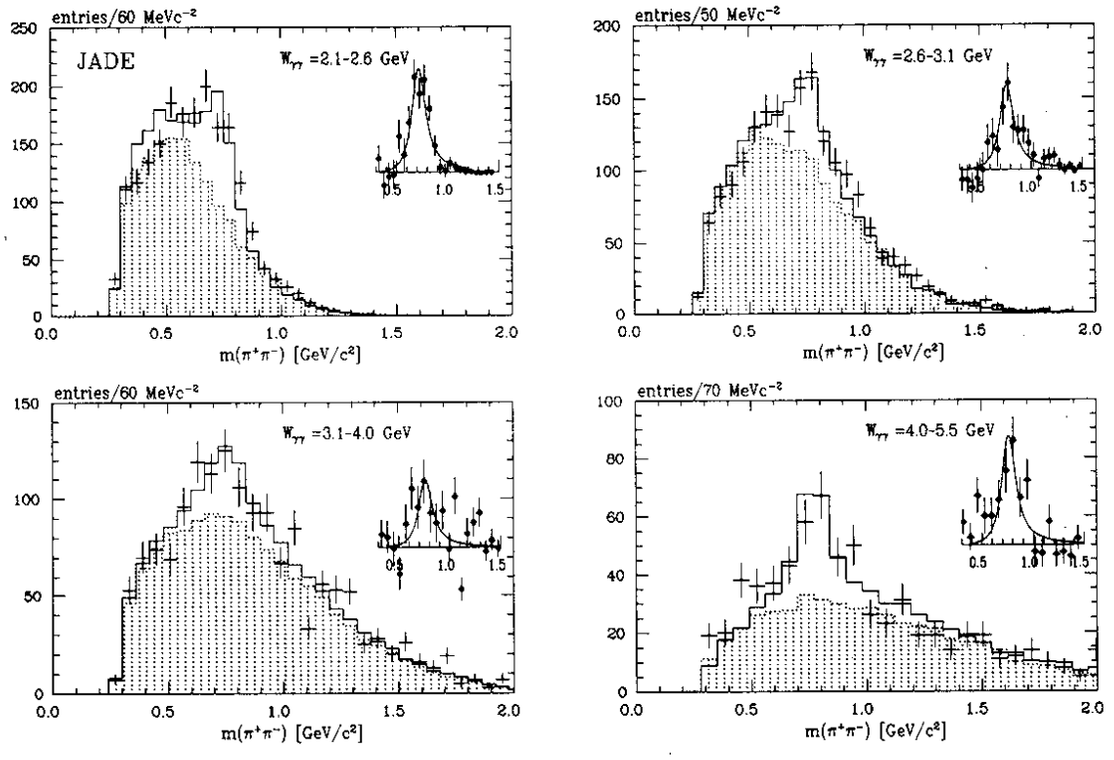

Figure 4: Fits to the $\pi^+\pi^-$ mass distribution (9 entries/event). The background distribution resulting from the non-resonant MC events is shown by the shaded histogram. The background subtracted data distribution is shown with the fitted Breit-Wigner curve in the insert. The MC distribution resulting from the ML fit is shown by the full histogram.

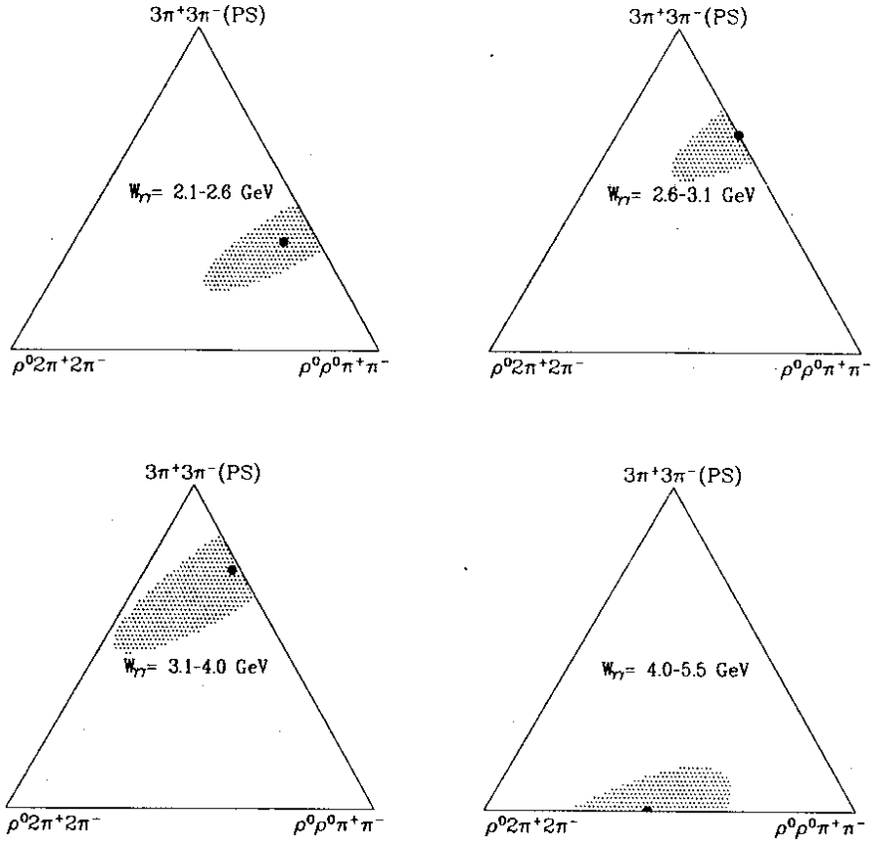

Figure 6: Fractions of the three processes $\gamma\gamma \to 3\,\pi^+\,3\,\pi^-$(phase space), $\gamma\gamma \to \rho^0 2\pi^+ 2\pi^-$ and $\gamma\gamma \to \rho^0\rho^0\pi^+\pi^-$, obtained by the extended maximum likelihood fit with incoherent weights in four different $W_{\gamma\gamma}$ bins. The points show the results listed in table 3 and the shaded areas give the 1 σ contours.

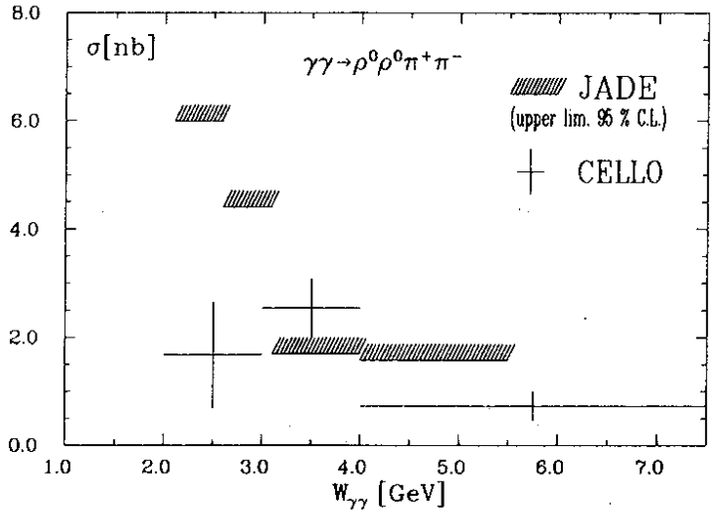

Figure 7: Upper limits for $\sigma(\gamma\gamma \to \rho^0\rho^0\pi^+\pi^-)$ in comparison with the result of the CELLO collaboration.

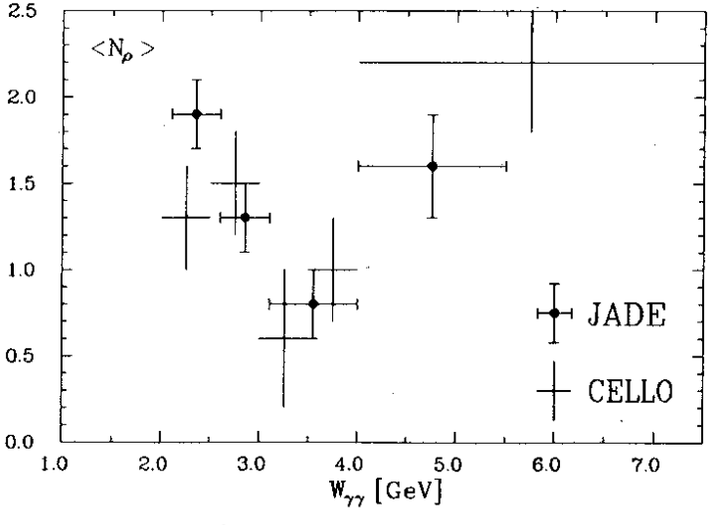

Figure 8: Average number of ρ^0's per event obtained by a χ^2 fit to the m($\pi^+\pi^-$) distribution. Comparison with the results of the CELLO collaboration.

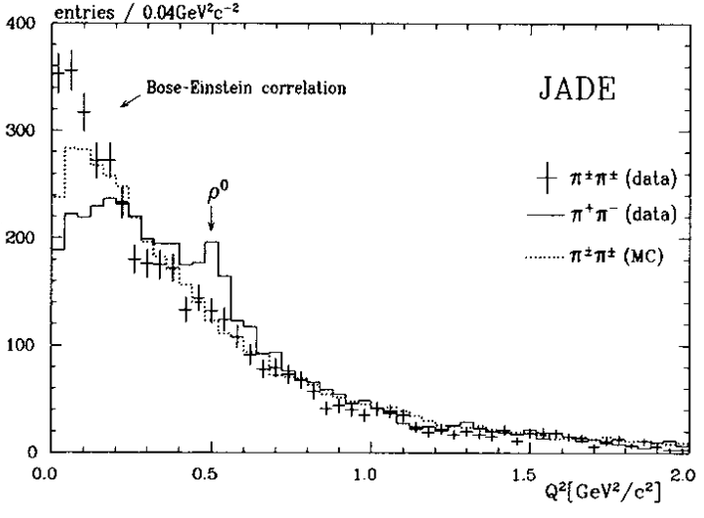

Figure 9: Number of like signed pion pairs compared with the reference samples. The MC simulation did not include the Bose–Einstein correlation.

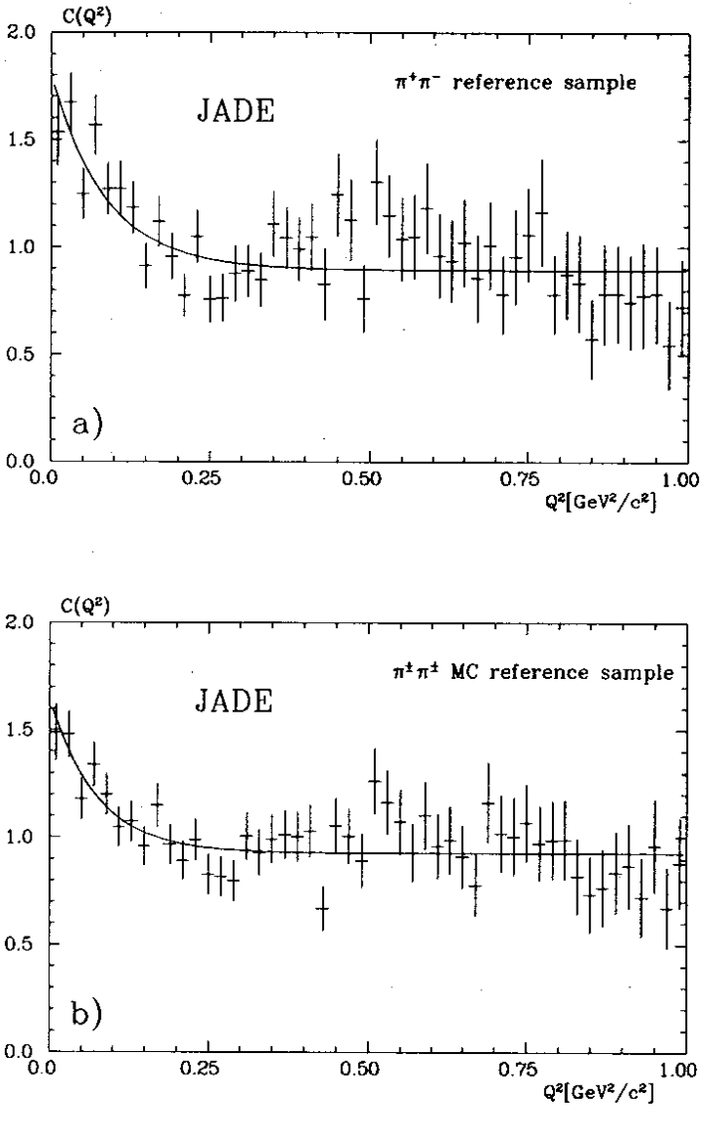

Figure 10: Fits to the Bose-Einstein correlation function. In a) the reference sample is the $\pi^+\pi^-$ distribution from the data, corrected for the ρ^0 contribution, in b) the MC $\pi^\pm\pi^\pm$ distribution is used as reference.